Applied Surface Science Advances 3 (2021) 100051

Contents lists available at ScienceDirect

Applied Surface Science Advances

journal homepage: www.elsevier.com/locate/apsadv

Explication of hydrophobic silica as effective pore former for membrane fabrication

Charlene Sharmini Fernandes[a], Nik Abdul Hadi Md Nordin[a,*], Muhammad Roil Bilad[a,b], Takeshi Matsuura[c], Zulfan Adi Putra[d], Mohd Dzul Hakim Wirzal[a], Juhana Jaafar[e]

[a] Department of Chemical Engineering, Universiti Teknologi PETRONAS (UTP), 32610 Seri Iskandar, Perak, Malaysia
[b] HICOE-Center of Biofuel and Biochemical Research, Institute of Self-Sustainable Building, Department of Chemical Engineering, Universiti Teknologi PETRONAS, Bandar Seri Iskandar 32610, Perak, Malaysia
[c] Industrial Membrane Research Laboratory, Department of Chemical and Biological Engineering, University of Ottawa, Ottawa, Ontario, Canada
[d] PETRONAS Group of Technical Solution, Project Delivery and Technology, Tower 3 KLCC, 50450 Kuala Lumpur, Malaysia
[e] Advanced Membrane Technology Research Centre (AMTEC), School of Chemical and Energy Engineering, Faculty of Engineering, Universiti Teknologi Malaysia (UTM), 81310 UTM Skudai, Johor Bahru, Malaysia

ARTICLE INFO

Keywords:
Phase inversion
Silica additive
Surface pore
Polyvinylidene difluoride
Membrane fouling
Liquid filtration

ABSTRACT

Membrane development is one of the key aspects to enhance the productivity of a filtration process. This study evaluates a hydrophobic silica as pore former for fabrication of polyvinylidene difluoride (PVDF) membrane for liquid based filtration and compare it with a hydrophilic silica. Membranes incorporated with hydrophobic (M-series) and hydrophilic silica (N-series) with loadings of 1, 2 and 3 wt% in the dope solution were fabricated, characterized and subjected to filtration tests using feeds of pure water, raw wastewater, secondary effluent, microalgae solution and activated sludge. Results show that the hydrophobic silica remained within the membrane matrix (7.24% of elemental Si by EDS), almost three-fold higher than the hydrophilic silica (2.48%). It turned the membrane surface to be more hydrophobic ascribed by increasing water contact angle from 87° from the pristine PVDF membrane up to 97° for the membrane with the highest loading of hydrophobic silica. On the other hand, the addition of hydrophilic decreased the contact angle down to 67° for the membrane with the highest loading. Loading hydrophobic silica enhanced the dope solution viscosities up to 1825–2000 cP, upon dropwise addition of nonsolvent (water), whereas the viscosity remained at 880–950cP for the hydrophilic silica. Addition of hydrophobic silica increased the number of surface pore without significantly altering the pore size of about 0.12 μm. On the other hand, an increase in the pore size (up to 0.33 μm) was observed when hydrophilic silica was added. Despite the smaller pore size, the pure water permeance of the hydrophobic silica loaded membranes (450–984 L/m^{2}hbar) outperformed the hydrophilic silica loaded membranes (420–600 L/m^{2}hbar) due to their higher surface porosities thanks to the higher number of surface pores. The filtration results of multiple feeds showed the advantages of loading more hydrophobic silica in improving the hydraulic performance. The findings demonstrate the efficacy of hydrophobic silica as pore former in PVDF membrane fabrication.

1. Introduction

The emerging membrane-based processes are considered as promising solutions for the treatment of water and wastewater. They are very attractive because of the higher separation efficiency, easy and automatic application, easy scale-up and low foot-print [1–3]. However, liquid based membrane filtrations are strongly limited by poor membrane intrinsic properties, as well as their propensity to lose performance overtime when handling fouling prone feeds. Membranes with a small number of pores operate at a high local-flux and susceptible to fouling [4–7], a situation highly undesirable as it increases cost of operation and would eventually reduce the membrane lifespan due to frequent intensive chemical cleaning to restore membrane performance [8,9].

One of the most common approaches to address the problems associated with performance loss is through membrane developments by turning the structure or surface chemistry often conducted during fabrication or via post treatment. Membrane development in the fabrication stage focuses on both achieving desirable surface chemistry as well as membrane morphology, often done by incorporating additives into the dope solution [10–13]. On the other hand, the post treat-

* Corresponding author.
E-mail address: nahadi.sapiaa@utp.edu.my (N.A.H. Md Nordin).

https://doi.org/10.1016/j.apsadv.2020.100051
Received 21 September 2020; Received in revised form 17 November 2020; Accepted 15 December 2020
Available online 22 December 2020

ment focuses on altering the membrane surface chemistry most commonly by improving wettability, as described in more detail elsewhere [14–16].

One of the most important factors that governs the membrane flux is the membrane surface characteristics, more specifically the number and the size of pores at the membrane surface [17–19]. The formation of membrane pore (number, size, distribution, etc.) is affected by polymer-solvent-nonsolvent interactions, polymer chain arrangement and entanglement that occur simultaneously during the initial stage of the phase inversion process [20,21].

The effect of the surface pores on membrane fouling can be explained in terms of the local-flux and the critical-flux. Local-flux is defined as the flux experienced by each individual pore [6], the sum of local-fluxes over the unit area of the membrane surface then becomes the reported operational flux. Membranes with more pores experience a lower local flux despite having a similar operational flux. It follows that each pore experiences lower specific hydraulic loading (low local-flux). This in turn reduces the drag force that carries the foulant materials into the pores. Consequently, it offers prolonged time for the membrane to reach the critical flux (the flux when membrane fouling becomes severe) and thus offer a more sustained operation [22].

Considering the importance of the porous morphological structure in sustaining the filtration, many studies have been carried out to develop highly porous membranes mostly via incorporation of pore forming additives into the casting dope, and recently via development of surface pattern [23–25]. Hydrophilic polymeric additives such as polyvinylpyrrolidone and polyethylene glycol are the most popular among others [11,26–28]. Hydrophilic additives destabilize the dope solution, which results in instantaneous demixing and thus promotes formation of highly porous membrane with less macrovoids [29,30]. It should be noted that excessive hydrophilic additives would promote the formation of large pores and thus diminish the membrane separation selectivity [7,31,32].

Silica particles are another group of attractive additives due to the possibility to alter their surface properties via surface functionalization [33]. Silica nanoparticles have also been used as the carrier and anchor for antifouling ligands such as polyethylene glycol and PEG in the polyvinylidene fluoride (PVDF) matrix. For example, blending of PEG-SiO_2 into the casting solution could reduce migration/leaching of PEG from PVDF matrix and enhance the wettability of the resulting membranes [34]. Loading of silica particles into dope solution significantly enhances solution viscosity, which allows to manipulate the membrane structure by enhancing the kinetic effect during the phase inversion [35,36]. Hydrophilic silica particles have been proven as favorable additives in suppressing formation of sponge-like structure and in enlarging membrane pore size, porosity and wettability [35,37]. However, loading of hydrophobic fumed silica did not significantly affect the pore size (when casted on non-woven support) but significantly enhanced the flux when tested in vacuum membrane distillation and for raw water filtration [38,36]. Thus, contrasting roles of hydrophobic and hydrophilic silica in affecting the membrane structure have been reported. However, only a limited number of reports are available that directly compare their roles as additives for membrane fabrication.

The objective of this study is to explicate the effect of hydrophobic silica as pore-forming additive for the fabrication of PVDF membranes and to compare with that of the hydrophilic silica. Detailed analyses of the relationship between the surface pore properties and the membrane performances were performed to unravel the roles of silica in enhancing surface pore formation and thus hydraulic performance. The analysis was based on the hypothesis that highly viscous dope solution in the presence of a small amount of hydrophobic silica would promote formation of a larger number of pores on the membrane surface, which eventually enhances the hydraulic performance. The performances of the developed membranes were then assessed for filtration of raw wastewater, secondary effluent, microalgae solution and activated sludge.

2. Experimental

2.1. Materials

PVDF (Sigma-Aldrich, MW=534 kDa by GPC), dimethylformamide (DMF, Sigma-Aldrich) and deionized water were used as the polymer, the solvent and the non-solvent, respectively. The hydrophobic silica additive used was the fumed silica nanoparticle (CAB-O-SIL of TS-610, CABOT EMEA Switzerland) surface modified with dimethyldichlorosilane and the hydrophilic silica additive used was the nano SiO_2 (MGS-E from Zhengzhou Dongshen Petrochemical Technology Co., Ltd). All chemicals were used as received without prior treatment or purification.

2.2. Membrane fabrication

A dope solution was prepared using PVDF, DMF and hydrophobic or hydrophilic silica as the polymer, solvent and additive, respectively. First, a predetermined amount of silica was added into the solvent and the suspension was stirred by a magnetic stirrer (Table 1). Then, 10% of the polymer was added slowly into the suspension for priming, followed by the addition of the remaining polymer slowly in 1% intervals. The stirring was continued until the polymer was completely dissolved. The polymer/solvent/additive suspension was further sonicated for 1–2 h to ensure complete dispersion of the silica particles before casting. The compositions of the dope solutions are summarized in Table 1.

The dope solution was casted on a non-woven support (Novatexx 2471, Freudenberg-Filter, Germany) to avoid excessive shrinkage [39] using a doctor blade at a wet casting thickness of 330 μm at room temperature (25 °C). The cast film was immediately immersed in a water bath where the polymer solidification took place. The membranes were kept immerse in coagulation bath until further usage. The membranes codes were the same as those of the casting dopes listed in Table 1.

2.3. Characterizations

Both hydrophobic and hydrophilic silica were characterized using a Fourier-transform infrared spectroscopy - attenuated total reflection (FTIR-ATR) to identify their surface functional groups. All spectra were recorded in the wavenumber range of 500–4000 cm^{-1}. The viscosity of the dope solutions was measured using a Brookfield CAP 2000 viscometer with spindles 6 and 9 at 900 rpm and a hold time of 20 s. Five different readings were taken for each viscosity measurement and the average recorded. Viscosity tests were also carried out via drop-wise addition of nonsolvent to the dope solution (both containing hydrophobic and hydrophilic) to comprehend the effect of nonsolvent influx to the cast film during the phase inversion. The original dope solution viscosity without addition of water demonstrated the impact of both types of silica in promoting viscosity. Simple dispersion tests were also carried out to confirm the hydrophobicity/hydrophilicity of the silica. 0.5 g of hydrophobic or hydrophilic silica nanoparticles were dispersed in 40 g of water and their agglomeration behavior was observed.

The surface and cross-sectional images of the membranes were obtained by a FESEM (Zeiss Supra 35VP FESEM Carl Zeiss, Inc., USA) with an accelerating voltage of 5 kV. For the cross-sectional image, the membrane was freeze fractured, followed by sputter coating with platinum. Energy dispersive X-ray spectroscopy (EDS) analysis was conducted for the Blank, N-3 and M-3 membranes to know the elemental composition of oxygen, carbon, fluorine and silica in the samples. The surface pore size distributions of Blank, M-3 and N-3 membrane were also obtained by ImageJ analysis according to the method described elsewhere [40]. The thickness of the resulting membranes of Blank, M-1, M-2 and M-3 were measured using micrometers.

The pore size and pore distribution were determined using a porometer (Porolux 1000, IB-FT GmbH, Germany). Membranes were immersed in Porefil® solution for 1 h prior to the analysis of the wet membrane

Table 1
Composition of the casting dope.

Membrane	PVDF (wt%)	DMF (wt%)	Hydrophobic silica (wt%)	Hydrophilic silica (wt%)
Blank (M-0)	15	85	–	–
M-1	14	85	1	–
M-2	12	85	2	–
M-3	11	85	3	–
N-1	14	85	–	1
N-2	12	85	–	2
N-3	11	85	–	3

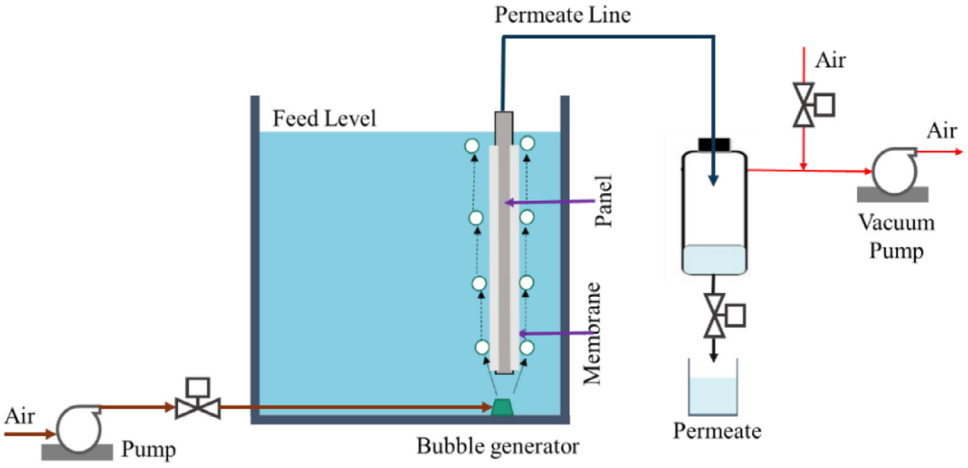

Fig. 1. Illustration of the submerged filtration set-up.

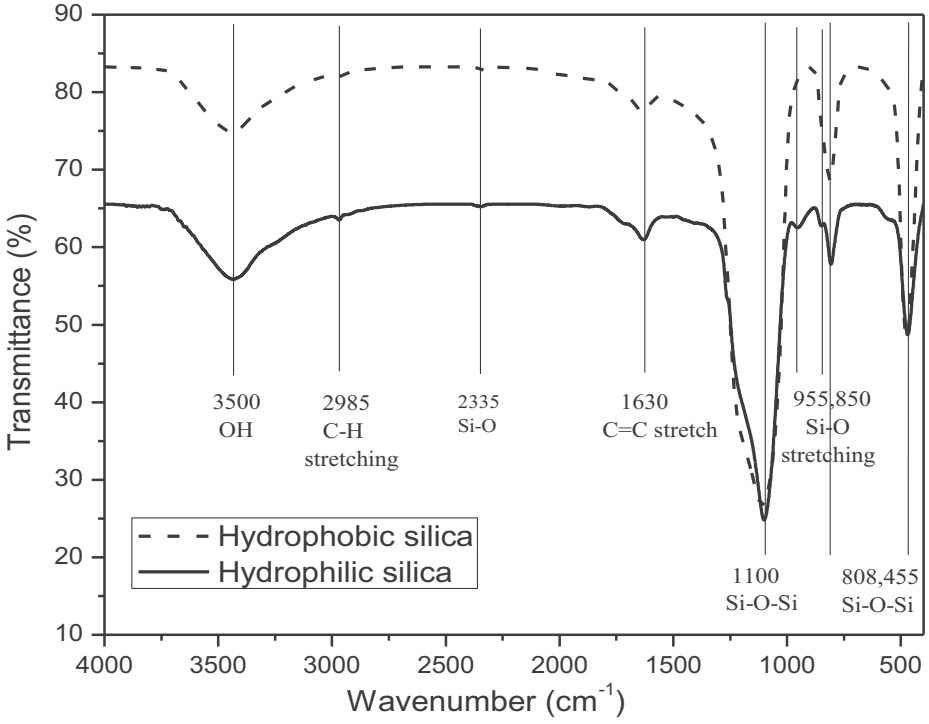

Fig. 2. FTIR spectra of the hydrophilic and the hydrophobic silica additives.

samples. The pressure range tested was between 0 and 6 bar with a 20 s stabilization timeout period.

The contact angle of each membrane surface was measured using a Goniometer (OCA 20, Data Physics) by the Sessile method at ambient temperature and humidity. A 7 μL of deionized water was dropped on the membrane surface by using a syringe and the image of the water droplet was captured by high-resolution camera and analyzed using the image-processing software (DSAI). The measurement was done at least five times at different spots of a sample and the results were averaged.

2.4. Filtration test

The filtration test of the membranes was conducted by a constant-pressure submerged filtration system (Fig. 1). The PVDF membrane was assembled into a working module with an effective membrane area of

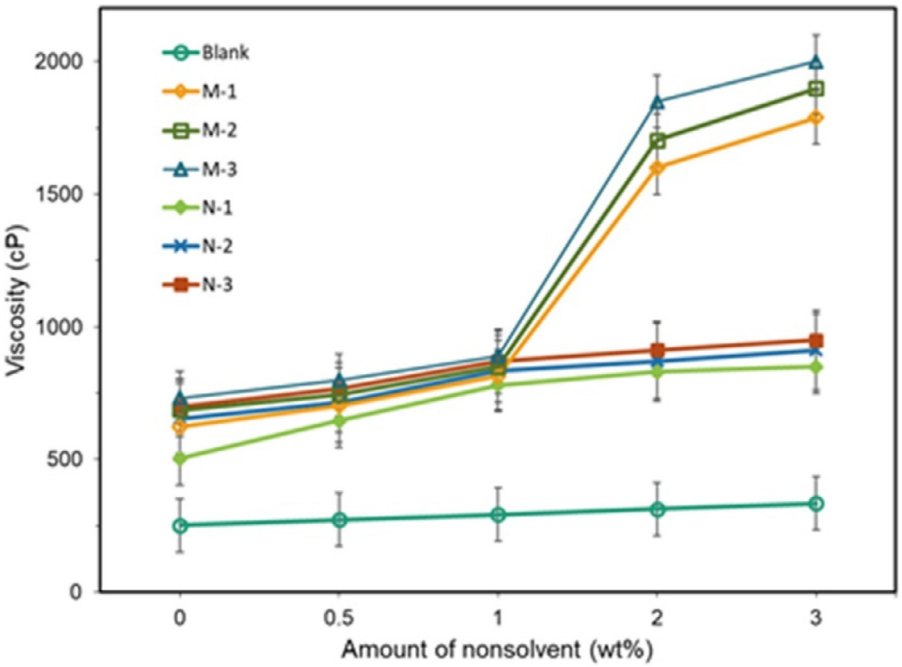

Fig. 3. Effect of drop-wise addition of water (nonsolvent) on the viscosity of the dope solutions.

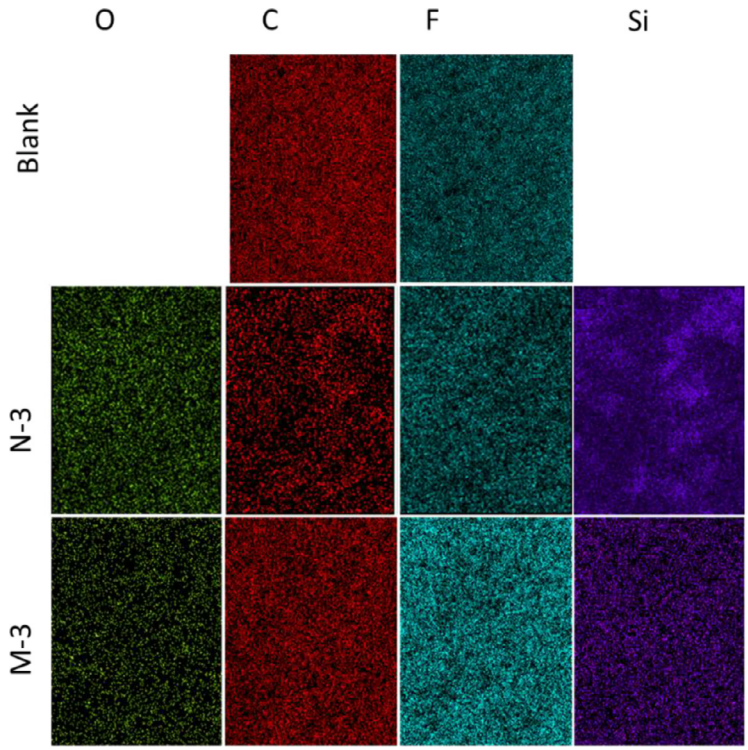

Element	Weight %	Atomic %
C K	37.39	48.58
F K	62.61	51.42
Totals	100.00	

Element	Weight %	Atomic %
C K	34.59	45.60
O K	3.50	3.47
F K	59.43	49.54
Si K	2.48	1.40
Totals	100.00	

Element	Weight %	Atomic %
C K	31.81	42.76
O K	8.07	8.14
F K	52.88	44.93
Si K	7.24	4.16
Totals	100.00	

Fig. 4. EDS mapping comparison of membranes with hydrophobic and hydrophilic silica additives. The insets show the relative compositions of elements.

0.012 m^2 (2-sided surface of four of 10 cm x 6 cm frame), and the module was immersed in a feed vessel of 5 L. A slight vacuum was applied on the permeate side of the membrane by an air pump to maintain the trans-membrane pressure (ΔP) constant at 0.1 bar. The permeate was collected every 10 min and weighed before it was returned to the feed vessel. An aeration system was installed, and air bubbles were supplied to the membrane surface constantly at a rate of 1 L/min to reduce the membrane fouling and concentration polarization.

The permeance (L, L/m^2hbar) and the rejection (R,%) were calculated by Eqs. (1) and (2), respectively.

$$L = \frac{V}{At\Delta P} \tag{1}$$

$$R = \frac{C_f - C_p}{C_f} x\ 100\% \tag{2}$$

where V is the permeate volume (L), A the effective membrane area (m^2), t the filtration time (h), ΔP the trans-membrane pressure (bar). C_f and C_p are the concentration in the feed and in the permeate (g/L), respectively. The permeate was subjected to the analysis after discarding the first 1 h collection of permeate, assuming that the steady state was

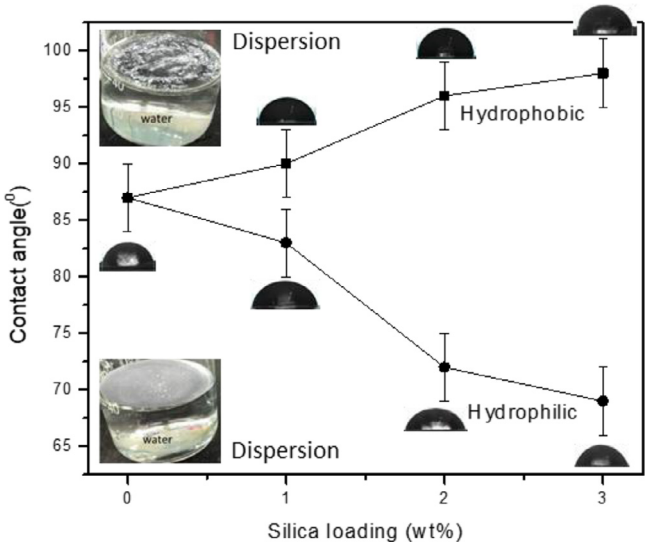

Fig. 5. Contact angle of all membrane samples as function of silica types and loadings. The insets show the magnified water droplet during the measurements and the picture of silica particles dispersion in water.

reached during this period, which typically reached within this duration as reported earlier [41]. Physical cleaning was applied in between filtration test by scrapping off the foulant and immersing the membrane in 0.08% NaOCl solution for one hour. Each filtration test was conducted trice and the result of permeability evolution overtime is presented as average value while the steady-state permeability was reported as average with standard deviation. It is worth noting that despite of the excellent chemical resistance of PVDF polymer under extreme pH [42,43], chemical treatment may affect the silica additives that still resided in the membrane matrix.

3. Results & discussion

3.1. Silica particles and membrane characterizations

3.1.1. FTIR of the silica particles

Fig. 2 shows the FTIR spectra detailing the functional groups present in both hydrophobic and hydrophilic silica particles. For both particles, peaks appear at C–H stretching (2985 cm^{-1}), C = C (1630 cm^{-1}), Si-O-Si (1100 cm^{-1}, 800cm^{-1} and 450 cm^{-1}) [44]. Two peaks at 953cm^{-1} and 955cm^{-1} are present for the hydrophilic silica but are absent for the hydrophobic silica. These two peaks refer to in-plane Si-O stretching [45]. Although a peak appear of Si-O-Si (1100 cm^{-1}, 800cm^{-1} and 450 cm^{-1}) vibration for both type of silica, the intensity is much stronger for the hydrophobic silica [44,45]. The two additives pose a contract of

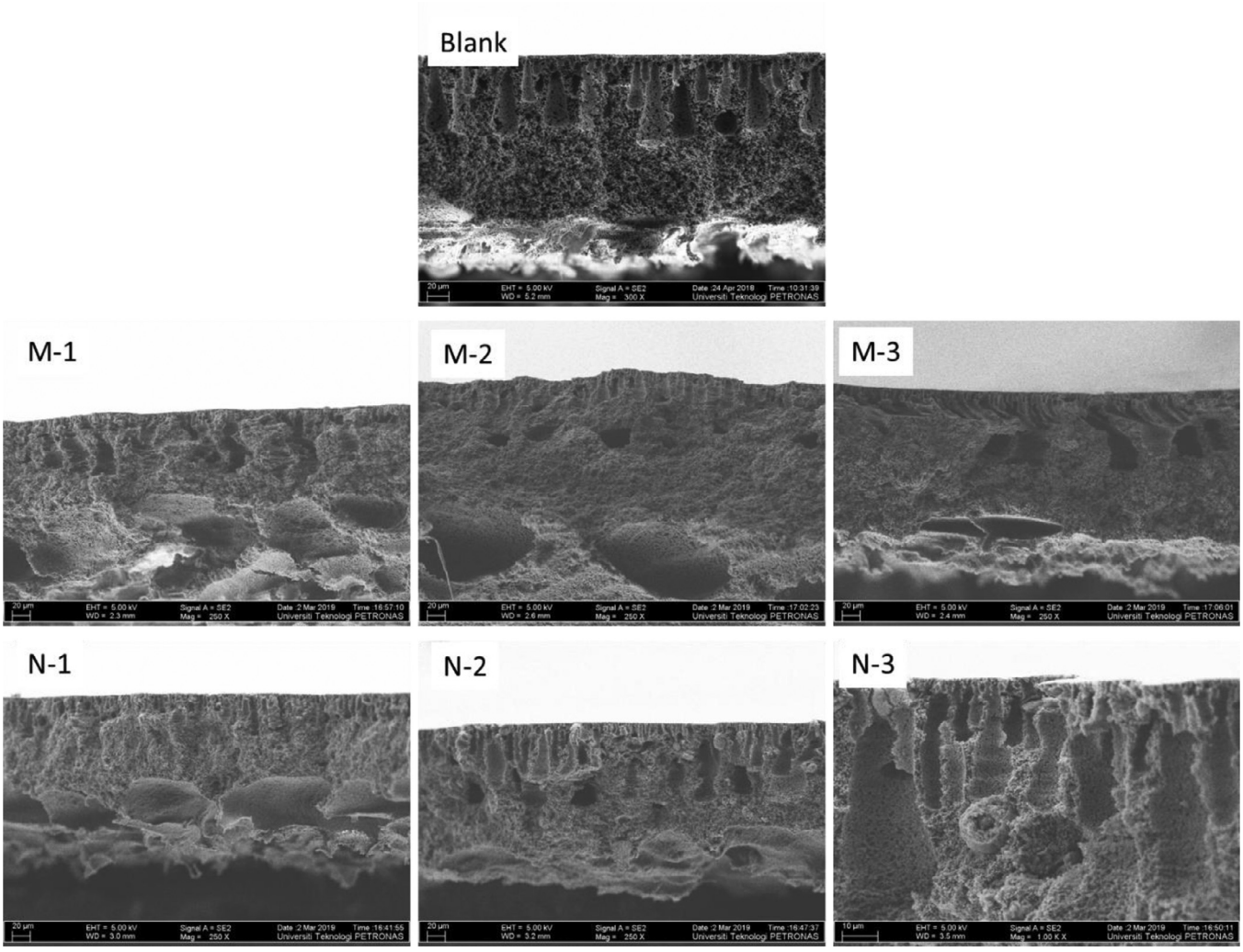

Fig. 6. Cross-section micrographs of all prepared membranes loaded with hydrophobic silica (M-series) and hydrophilic silica (N-series).

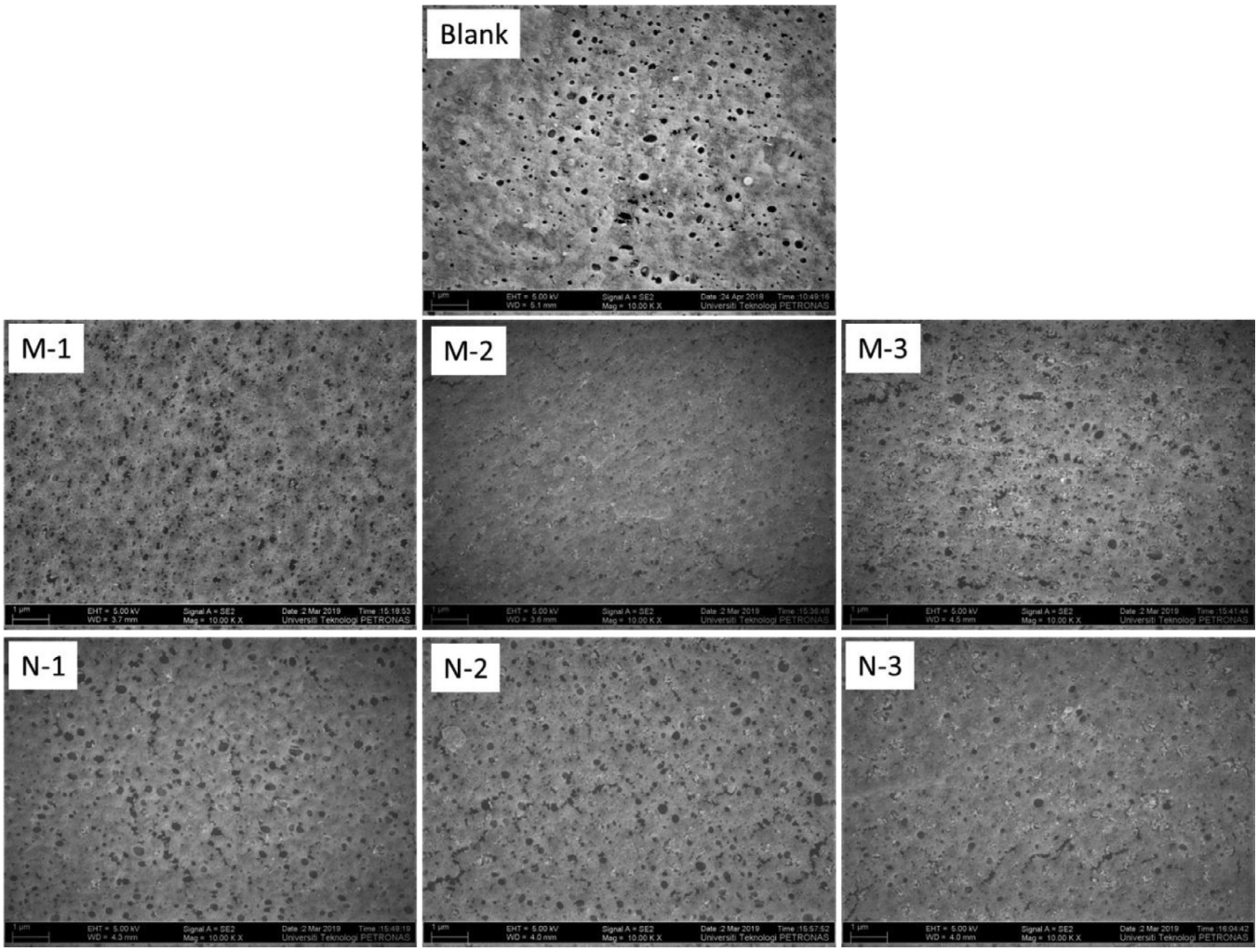

Fig. 7. FESEM surface micrographs of all prepared membranes loaded with hydrophobic silica (M-series) and hydrophilic silica (N-series).

hydrophobicity and their effects on the resulting membrane properties are thus expected.

3.1.2. Impact of the silica particles on viscosity

The results of viscosity measurements are presented in Fig. 3 showing that the viscosity increases upon addition of silica nanoparticles for both the hydrophobic and the hydrophilic. Upon dropwise introducing the nonsolvent (water), the difference between hydrophobic (M-series) and hydrophilic silica (N-series) was insignificant until the nonsolvent concentration exceed 1 wt.%, indicating similar polymer chain entanglement. Beyond 1 wt.%, however, viscosity increases steeply for the M-series, while modest viscosity increment is shown for the N-series. These results suggest that hydrophobic silica induce sudden polymer entanglement due to its low affinity towards water, thus leads to sudden increase in the dope solution viscosity. Polymer entanglements are expected to be more prominence in the presence of water during the phase inversion. Consequently, it leads to slower demixing because of the rheological properties of the polymer that slows down the exchange of solvent and nonsolvent during the phase inversion. Such rheological phenomenon plays significant role on the surface pore formation, as demonstrated in Section 3.2. High viscosity induced by the hydrophobic additive provide rheological hindrance for the solvent and nonsolvent exchange during the phase inversion that leads to formation of more abundance number of surface pores.

3.1.3. Amount of silica left in the membrane

Fig. 4 shows the EDS mapping for Blank, M-3 and N-3 membranes showing relative elemental composition near the top of the membrane surface. The O and Si elements appear in M-3 and N-3, indicating the presence of silica nanoparticles. Comparatively, elemental silicon content are 7.24% and 2.48% for M-3 and N-2, respectively. Higher silicon content of M-3 can likely be attributed to the steep increase in the dope solution viscosity with an increasing amount of the added water, which slowed down the motion of the particles from the polymer matrix toward the water bath. On the other hand, the affinity between hydrophilic particles and water enhanced the particle motion, resulting in less particle embedding in the membrane. Moreover, the hydrophobic silica is homogeneously distributed compared to the hydrophilic silica, as also reported elsewhere [38] and thus confirms the compatibility of the fumed silica and the PVDF from theoretical analysis using Hansen's solubility parameter [36].

Dispersion test results shown in the insets of Fig. 5 indicates that hydrophilic silica has a high affinity towards water which was used as the nonsolvent, which promotes leaching of hydrophilic silica from the cast film. On the other hand, hydrophobic silica loaded in the membrane matrix exhibited minimal leaching ascribed from its low affinity towards water.

3.1.4. Water contact angle and membrane thickness

Fig. 5 shows the results of the contact angle measurement. The contact angle increases progressively with an increase in hydrophobic silica

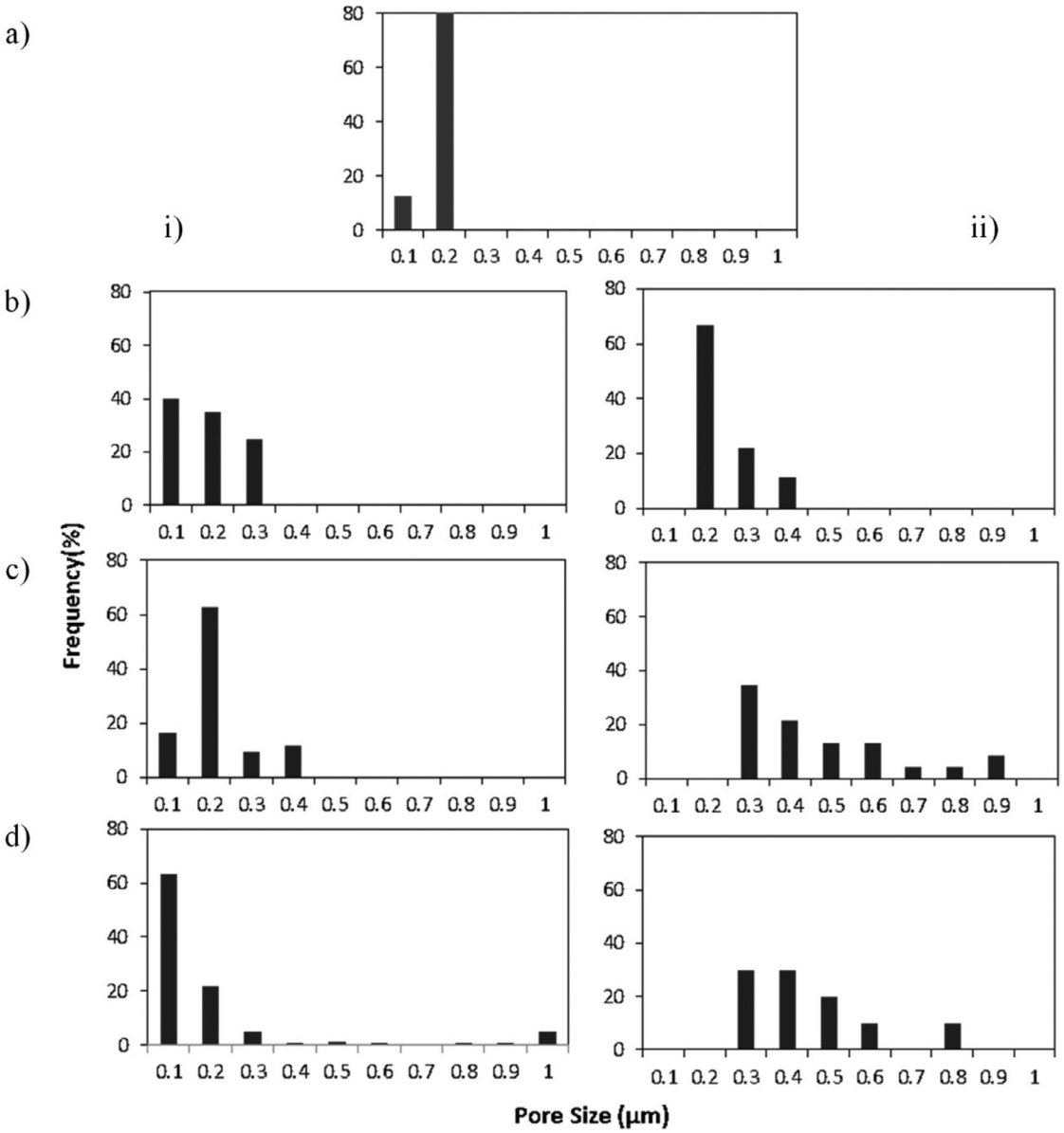

Fig. 8. Histogram of pore size distributions of the membrane samples indicating a) blank, b) 1 wt%, c) 2 wt%, and d) 3 wt%, while i) denotes the ones loaded with the hydrophilic silica (N-series) and ii) denotes the ones loaded with the hydrophobic silica (M-series).

loading (M-series), while the trend is opposite for the hydrophilic loading (N-series). Similar trends were also reported by others [35–37].

Dosing of the hydrophobic additive into the dope solution lead to an increment in the resulting membrane thickness. The thickness of M-0 is 210.0 ± 1.6, significantly lower than the hydrophobic silica loaded membranes that pose the thicknesses of 224.8 ± 0.8, 237.8 ± 2.4 and 220.6 ± 5.9 for M-1, M-2 and M-3, respectively. The thickness property is associated with the rate of solvent and non-solvent exchange during the phase inversion. The high thickness of the M-series membranes can be attributed to the high viscosity of the dope solution that limits the transport of the solvent from the film to the bulk of the coagulation bath. Nonetheless, after reaching certain viscosity (for dope solutions of M1, M2 and M-3), the impact seems diminishing from inconclusive trend of thickness of the M-series membranes.

3.1.5. Membrane morphology

The impact of the sudden increase in dope solution viscosity on the membrane structure is demonstrated by the overall cross-sectional image of the resulted membranes (Fig. 6). Increasing hydrophobic silica (M-series) loading suppresses the fingerlike structure as compared to the corresponding hydrophilic counterpart (N-series). This means that the hydrophobic silica induces slower demixing as also confirmed by others [37]. Blank membrane possesses an asymmetric structure with fingerlike and sponge-like supporting sub-structure.

When comparing M-1 and N-1, the fingerlike suppression is prominent even at low loading (1 wt.%) of hydrophobic silica, since the enhancement of dope solution viscosity is noticed even at silica loading of 1 wt.% (Fig. 3). On the other hand, as the hydrophilic silica loading increases from N-1 to N-3 the fingerlike structure becomes increasingly dominant, indicating the acceleration of demixing by the hydrophilic silica. This finding demonstrates the contrasting effect of hydrophobic and hydrophilic silica on the phase inversion process in which the former promotes delayed demixing, while the latter induces instantaneous demixing.

The surface morphologies of all prepared membranes are shown in Fig. 7 to depict the population and size of the surface pores. Higher loading of the hydrophobic silica significantly increases the number of surface pores for the M-series membranes. Similar trend was also re-

ported by Baghbanzadeh et al. which clearly demonstrated the increasing number of surface pores from the ImageJ analysis of the surface SEM images [38]. Interestingly, the size of the surface pores in the M-series membranes does not change much with increasing loading, which was also observed by Mavukkandy et al. [36] by using the porometer. This observation suggests the role of the hydrophobic silica to increase the number of pores while maintaining the pore size nearly constant, as a result of slowed phase inversion. In contrast, for the N-series membranes the number of surface pores reduces with the increase of the hydrophilic silica loading while the pore size increases from N-0 to N-1, whereas membranes N-2 and N-3 have large and almost equal pore sizes.

3.2. Membrane pore and pore formation mechanism

3.2.1. Pore size distribution

The histograms of pore size distribution from capillary porometer measurement for all prepared membranes area shown in Fig. 8. The general trends observed in Fig. 8 are as follows:

i The blank PVDF membrane has almost 80% of pores with sizes ranging from 0.1 to 0.2 μm and 10% of pores <0.1 μm.
ii As for M-series, M-1 and M-2 have distribution on both sides of the range from 0.1 to 0.2 μm, while in M-3 the distribution shifts to the lower pore size range, showing 61% of pores in the range < 0.1 μm.
iii As for N-series, the distribution spreads wider toward larger pore sizes from N-1 to N-2. The pore size distribution of N-3 looks similar to that of N-2.

Overall, addition of hydrophobic silica tends to reduce the pore size, whereas the addition of hydrophilic silica tends to increase the pore size. As well, comparing M-series with N-series, the distributions of all N-series are on the larger pore size ranges (>0.1 μm).

3.2.2. Mean flow pore size

Fig. 9 summarizes the mean flow pore sizes of the membranes using capillary flow porometer. These results generally confirm the trends observed in Fig. 8. As for M-series, the change in pore size is insignificant from Blank to M-2. The pore size increases from M-2 to M-3, contrary to the trend shown in Fig. 8. These contrary observations can probably be ascribed to the pore size terminology measured by the two different methods. For example, if the small indents, which are counted as pores in the ImageJ analysis, are not penetrating through the membrane cross-section, they are not considered as pores in the porometer. As for N-series, the increasing trend of pore size with an increase in hydrophilic silica is also observed in Fig. 9. As well, the pore sizes of N-series membranes are larger than those of corresponding M-series membranes.

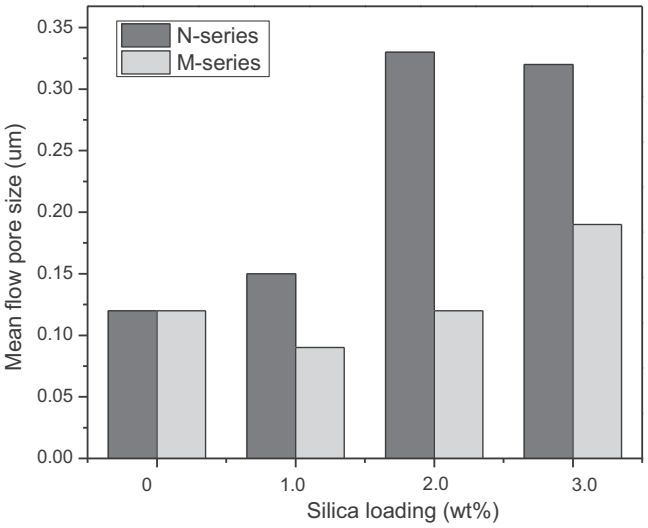

Fig. 9. Mean pore size data of all membrane samples.

The mean pore size data obtained are in line with the observation gathered from the membrane surface morphological images (Fig. 7), where the N-series membranes exhibited larger pore sizes on the membrane surface as compared to the M-series. This corresponds to the proposed theory that the hydrophobic silica promotes a higher number of pores on the surface but with smaller sizes. It is worth noting that a close observation on pair of M-2 and N-2 seems to contradict the claim. It occurs because of the poor visibility of surface pore in M-2 that has pore size of almost a half of the N-2 (See Fig. 9).

3.2.3. Surface porosity

The flux of a membrane is governed not by the pore size but by the porosity (total area of pores/area of the membrane). A membrane with a high surface porosity thus offers better fouling resistance [46]. The porosity was measured by ImageJ analysis for Blank, M-3 and N-3 membranes using the data on the number of pores and the pore size according to method detailed elsewhere [35]. The latter two membranes

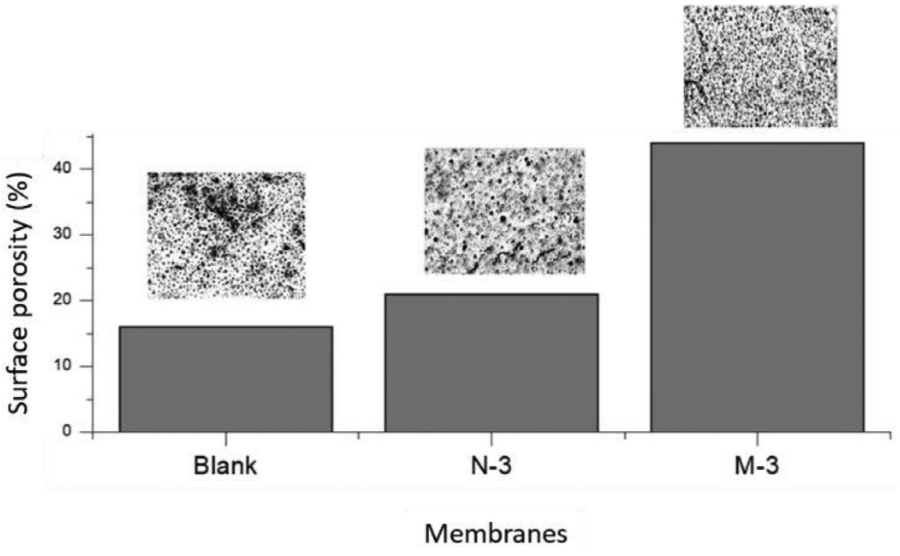

Fig. 10. Surface porosity of membranes. The insets show binary type of the surface SEM images of the corresponding membranes in which the black areas represent the surface pore.

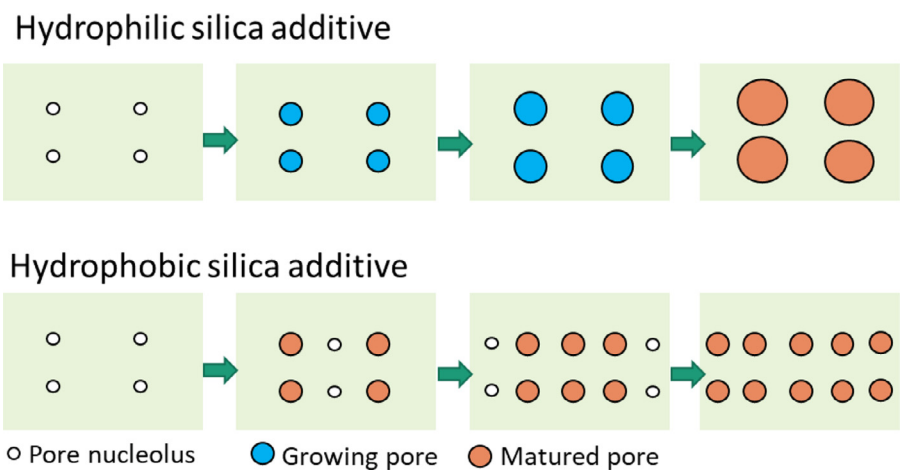

Fig. 11. Illustration of the surface pores formation mechanisms of on the cast film prepared from dope solution loaded with hydrophobic and hydrophilic silica.

were chosen to represent the effect of hydrophobic and hydrophilic silica additives.

Fig. 10 shows that the porosity increases from Blank to both M-3 and N-3 and the porosity of M-3 is much larger than that of N-3, despite the smaller pore sizes of M-3, as shown in Figs. 8 and 9. This is because the larger number of surface pores in M-3, as revealed by the SEM surface images shown in Fig. 3. These results imply that both solute rejection and flux of M-3 will be greater than N-3.

3.2.4. Role of hydrophobic additive on pore formation mechanisms

Fig. 11 illustrates the surface pore formation of the membranes as consequences of the silica loadings. It is a graphical illustration of our hypothesis on the surface pore formation mechanisms to depict the contrasting effect of the hydrophilic and hydrophobic silica additives, solution viscosity and the stages in pore nucleation, growth and maturation. Pore size enlargement agrees well with the demixing rates and correlates inversely with the cast film viscosity.

For the hydrophilic silica additive, upon formation of pore nucleus the pore size grows promoted by the fast demixing process, which is accelerated by the strong interaction of the additive with the water. The size of the pore continues growing until it forms mature size to stop. In Fig. 11, the growth of the surface pore is illustrated in three stages before it reaches the matured size. The pore growth is stopped due to the cast film viscosity reaching the gel point, in which the structure of the cast film is immobile and no further growth of pose size possible.

On the other hand, upon the presence of the hydrophobic additive, the growth of pore size is limited by the high viscosity of the dope solution and the strong interaction of the hydrophobic additive with the PVDF for the M-series membranes. This way, the formed pore size in the matured stage is relatively smaller than the one with hydrophilic additive. However, since for the system with similar polymer concentration and additives loadings, the restricted pore growth is compensated with formation of more pores in order to accommodate the solvent evacuation. As illustrated in Fig. 11, after the first batch of the pore nucleuses matured, new pore nucleuses are then formed and matured in the following stages and so on, until no pore nucleus can be formed. Combination of restricted pore growth and new pore formation resulting membrane with smaller pores and high porosity as observed in Fig. 10.

3.3. Hydraulic performance

Fig. 12 shows that pure water permeance (PWP) for all M- and N-series membranes. As expected in Section 3.2.3, M-series exhibited higher PWP than N-series membranes for a given particle loading. The difference in PWP of M-1 and N-1 was small (30 L/m^2 h bar), but the difference grew with an increase in loading, i.e. at 3 wt.% loading, PWP of M-3 and N-3 were 894 L/m^2 h bar and 600 L/m^2 h bar, respectively.

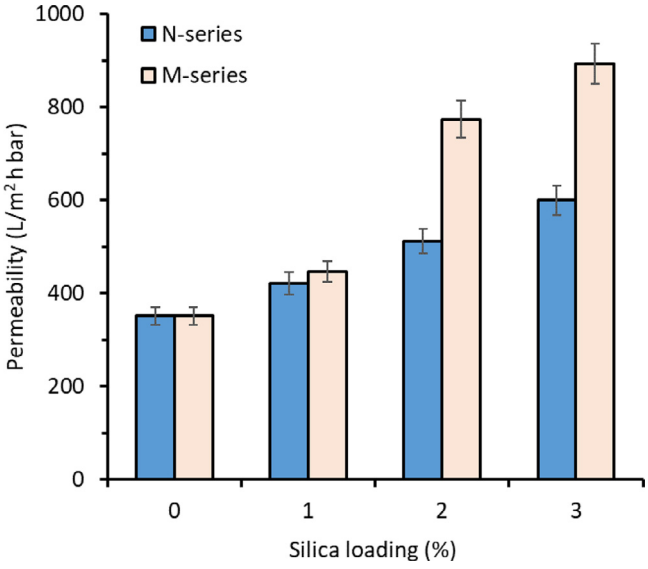

Fig. 12. Pure water permeability for all prepared membranes.

The increase of PWP at higher hydrophilic silica loading is attributed to the increase of pore size (Fig. 9) and high hydrophilicity (Fig. 5), while the increase of PWP at higher hydrophobic silica (M-series) loadings is attributed to the increase of the number of pores (Fig. 10), despite the decrease in pore size (especially for M-2). This result indicates that the number of pores and the overall porosity have greater influence on PWP than the pore size and hydrophilicity. Due to the higher PWP, only M-series membranes are subjected hereafter to the fouling filtration tests.

The effect of the pore size on flowrate could be studied via combining the Hagen-Poiseuille and the Darcy equation as in Eq. (3) [47].

$$\frac{Q}{\Delta P A} = L = \frac{\varphi r^2}{8 \mu l} \tag{3}$$

where Q is the flow rate (m^3/s), A the membrane area (m^2), L permeability (m/s), r the pore radius (m), μ the viscosity of liquid in pore (cP or kg/m/s), φ the surface porosity of the membrane (-) and l the length of the flow path (m). Eq. (3) shows that as the permeability is directly proportional to pore size, pore number and surface porosity.

Fig. 13 shows the filtration performance of all M-series membranes with secondary effluent, domestic wastewater, activated sludge and microalgae medium as the feeds over three filtration cycles. The four feeds were deliberately selected to envisage the universality of the trend. The membranes loaded with higher hydrophobic silica achieved much

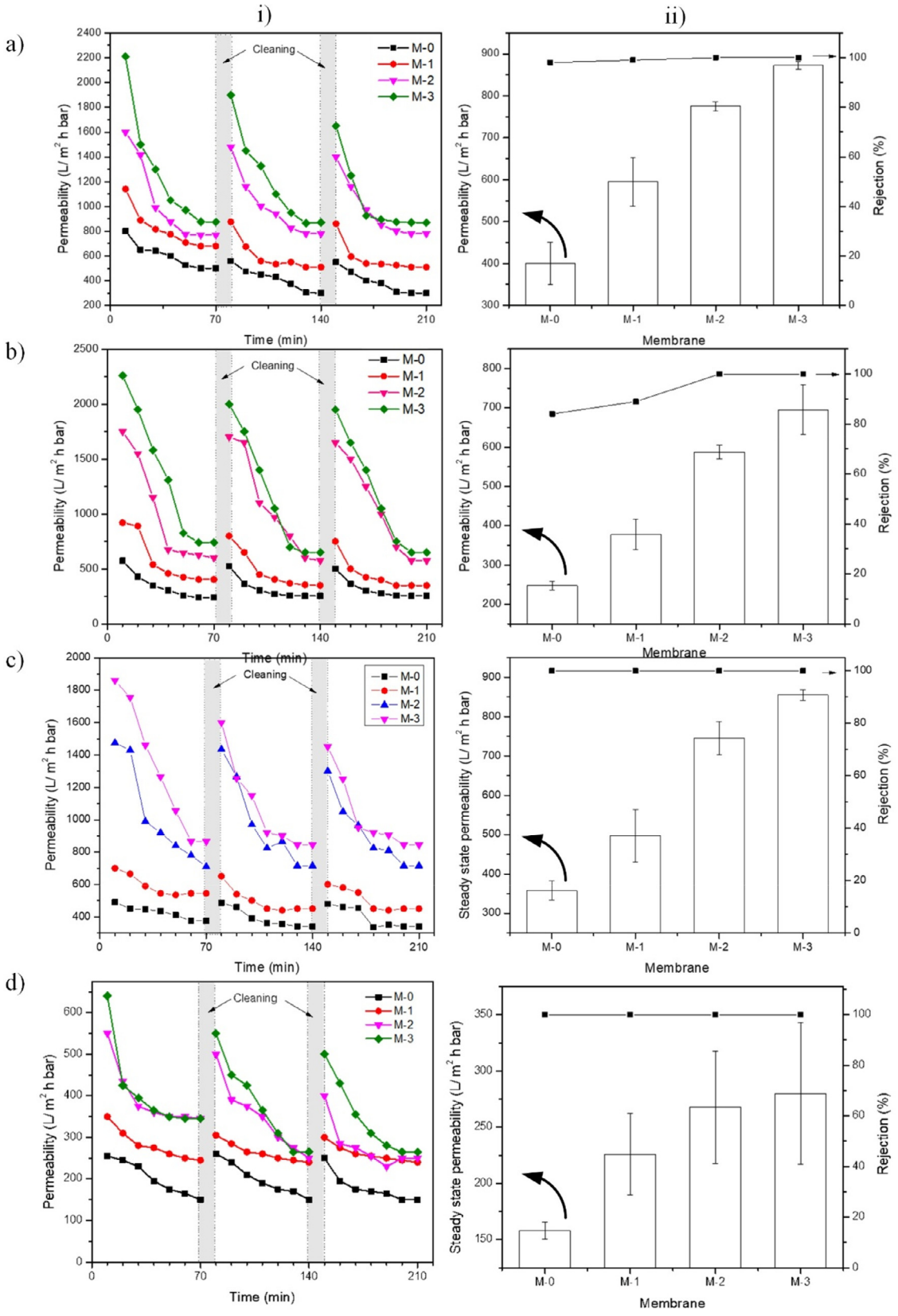

Fig. 13. Filtration performances of M-series membranes for treating different feeds: a) secondary effluent, b) domestic wastewater, c) activated sludge and d) *Euglena sp.* broth. Medium. i) denotes the permeance change over 3- filtration cycles and ii) denotes steady-state permeance at the end of 3- filtration cycle.

higher permeances for all tested feeds, e.g., the permeance of Blank and M-3 for filtration of secondary effluent, domestic wastewater, activated sludge and microalgae solution are 400 and 872, 247 and 695, 358 and 855 and 158 and 280 L/m^2 h bar, respectively, at the steady state (at the end of the 3rd cycle.) Such results are obviously convincing to demonstrate the efficacy of hydrophobic silica in enhancing membrane filterability. The level of enhancements varies as function of the feeds and this most likely due to their different membrane fouling propensity, which is beyond the scope of this study.

The main concern for the application of the developed membrane is on the potential of 'hydrophobic interaction' between the pollutant and membrane surface which can lead to severe membrane fouling [48]. Fig. 13 shows that the M-series membranes show superior permeability compared to Blank. Despite showing the largest drop in permeability over time, M-3 still exhibits the highest permeance. This means that foulant-membrane interactions effect is undermined by the larger number of surface pore available for permeate to pass through. Larger number of pores on the membrane surface would create higher number of water pathways, which can reduce the local flux thus reduce the effect of membrane fouling [6]. The results from the filtration cycles revealed that the membranes were able to recover its permeances, indicating the absence of irreversible fouling despite of its hydrophobic nature.

Detailed study on long-term fouling was not conducted in this study. However, the membrane fouling phenomenon for the M-series membrane can be deduced from the steady state permeability data presented in Fig. 13. The steady state permeability data are highly reproducible, except for the filtration of Euglena sp. broth. High reproducibility indicates that the fouling type was mostly reversible, with small fraction of irrecoverable fouling for all tested membranes. Nevertheless, detailed study on the anti-fouling properties of the membrane shall be the focus of future study. The positive role of hydrophobic silica in governing pore-rich polymer matric can be combined with chemical modification that imposes hydrophilicity to enhance the long-term antifouling property of the membranes.

The rejection and fouling test on N-series membrane were not done because the study was focused on the role of hydrophobic silica additive in enhancing the structural properties of the resulting membranes. Additional N-series membrane were made to demonstrate the contrast of hydrophobic vs hydrophilic additive. Nevertheless, since the feeds and the foulant materials were mostly particles or living cells, the smaller pore sizes of M-series membranes suggest they offer better rejection that the N-series membranes.

4. Conclusion

This study explicates the role of hydrophobic and hydrophilic silica particles as the additive for PVDF membrane fabrication. The following conclusions were drawn from the experimental results.

1 Both hydrophobic and hydrophilic silica leached out upon immersion of the cast film into the gelation bath. But the residual hydrophobic silica was three-fold higher than the hydrophobic silica in the membrane matrix.
2 The viscosity of the dope solution increased significantly in the presence of water when hydrophobic silica was added, whereas the viscosity did not increase when hydrophilic silica was added.
3 Addition of hydrophobic silica caused an increase in the number of pores while the pore size either remained unchanged or slightly decreased compared to the Blank membrane. This finding can be attributed to the increase of viscosity and the consequent slow demixing, which limits the growth of polymer lean phase. On the other hand, an increase in the pore size was observed when hydrophilic silica was added.
4 The surface porosity was higher for the M-series than the N-series membranes leading to the higher PWP of the M-series membranes.
5 The filtration experiments with secondary effluent, raw wastewater, activated sludge and microalgae solution showed that the hydrophobic silica added membranes could maintain their significantly higher fluxes than the pristine PVDF membrane (Blank) even after 3 filtration cycles.

Declaration of Competing Interest

The authors declare no conflict of interest.

Acknowledgment

The first author acknowledges the financial support provided by Universiti Teknologi PETRONAS under graduate assistance scheme and AMTEC Fellowship Awarded in 2018 under HICOE Grant (A.J090301.5300.07092). The research was funded by Fundamental Research Grant Scheme of Ministry of Higher Education (grant number: 015MAO-039).

References

[1] A.F. Ismail, T. Matsuura, Sustainable Membrane Technology for Energy, Water, and Environment, John Wiley & Sons, 2012.
[2] R.W. Baker, Membrane Technology and Applications, 3rd edition, John Wiley & Sons, Chichester, West Sussex, U.K., 2012 http://proxy2.hec.ca/login?url=http://library.books24x7.com/library.asp?B&bookid=49678 (accessed September 26, 2013).
[3] M.R. Bilad, H.A. Arafat, I.F.J. Vankelecom, Membrane technology in microalgae cultivation and harvesting: a review, Biotechnol. Adv. 32 (2014) 1283–1300, doi:10.1016/j.biotechadv.2014.07.008.
[4] P. Bacchin, B. Espinasse, P. Aimar, Distributions of critical flux: modelling, experimental analysis and consequences for cross-flow membrane filtration, J. Membr. Sci. 250 (2005) 223–234, doi:10.1016/j.memsci.2004.10.033.
[5] P. Bacchin, A. Marty, P. Duru, M. Meireles, P. Aimar, Colloidal surface interactions and membrane fouling: investigations at pore scale, Adv. Colloid Interface Sci. 164 (2011) 2–11, doi:10.1016/j.cis.2010.10.005.
[6] S. Ognier, C. Wisniewski, A. Grasmick, Membrane bioreactor fouling in sub-critical filtration conditions: a local critical flux concept, J. Membr. Sci. 229 (2004) 171–177, doi:10.1016/j.memsci.2003.10.026.
[7] P. van der Marel, A. Zwijnenburg, A. Kemperman, M. Wessling, H. Temmink, W. van der Meer, Influence of membrane properties on fouling in submerged membrane bioreactors, J. Membr. Sci. 348 (2010) 66–74, doi:10.1016/j.memsci.2009.10.054.
[8] A. Piasecka, R. Bernstein, F. Ollevier, F. Meersman, C. Souffreau, R.M. Bilad, K. Cottenie, L. Vanysacker, C. Denis, I. Vankelecom, Study of biofilms on PVDF membranes after chemical cleaning by sodium hypochlorite, Sep. Purif. Technol. 141 (2015) 314–321, doi:10.1016/j.seppur.2014.12.010.
[9] C. Regula, E. Carretier, Y. Wyart, G. Gésan-Guiziou, A. Vincent, D. Boudot, P. Moulin, Chemical cleaning/disinfection and ageing of organic UF membranes: a review, Water Res. 56 (2014) 325–365, doi:10.1016/j.watres.2014.02.050.
[10] L. Marbelia, M.R. Bilad, S. Maes, H.A. Arafat, I.F.J. Vankelecom, Poly(vinylidene fluoride)-based membranes for microalgae filtration, Chem. Eng. Technol. 41 (2018) 1305–1312, doi:10.1002/ceat.201700622.
[11] I.-.C. Kim, K.-.H. Lee, Effect of various additives on pore size of polysulfone membrane by phase-inversion process, J. Appl. Polym. Sci. 89 (2003) 2562–2566, doi:10.1002/app.12009.
[12] M. Sadrzadeh, S. Bhattacharjee, Rational design of phase inversion membranes by tailoring thermodynamics and kinetics of casting solution using polymer additives, J. Membr. Sci. 441 (2013) 31–44, doi:10.1016/j.memsci.2013.04.009.
[13] G.R. Guillen, Y. Pan, M. Li, E.M.V. Hoek, Preparation and characterization of membranes formed by nonsolvent induced phase separation: a review, Ind. Eng. Chem. Res. 50 (2011) 3798–3817, doi:10.1021/ie101928r.
[14] M.M. Nasef, O. Güven, Radiation-grafted copolymers for separation and purification purposes: status, challenges and future directions, Prog. Polym. Sci. 37 (2012) 1597–1656, doi:10.1016/j.progpolymsci.2012.07.004.
[15] D.J. Miller, D.R. Dreyer, C.W. Bielawski, D.R. Paul, B.D. Freeman, Surface modification of water purification membranes, Angew. Chem. Int. Ed. 56 (2017) 4662–4711, doi:10.1002/anie.201601509.
[16] N. Nady, M.C.R. Franssen, H. Zuilhof, M.S.M. Eldin, R. Boom, K. Schroën, Modification methods for poly(arylsulfone) membranes: a mini-review focusing on surface modification, Desalination 275 (2011) 1–9, doi:10.1016/j.desal.2011.03.010.
[17] A.G. Fane, C.J.D. Fell, A.G. Waters, The relationship between membrane surface pore characteristics and flux for ultrafiltration membranes, J. Membr. Sci. 9 (1981) 245–262, doi:10.1016/S0376-7388(00)80267-7.
[18] M. Gryta, Influence of polypropylene membrane surface porosity on the performance of membrane distillation process, J. Membr. Sci. 287 (2007) 67–78, doi:10.1016/j.memsci.2006.10.011.
[19] R. Ziel, A. Haus, A. Tulke, Quantification of the pore size distribution (porosity profiles) in microfiltration membranes by SEM, TEM and computer image analysis, J. Membr. Sci. 323 (2008) 241–246, doi:10.1016/j.memsci.2008.05.057.

[20] P. Vandezande, L.E.M. Gevers, I.F.J. Vankelecom, Solvent resistant nanofiltration: separating on a molecular level, Chem. Soc. Rev. 37 (2008) 365–405, doi:10.1039/B610848M.
[21] Z. Zhenxin, T. Matsuura, Discussions on the formation mechanism of surface pores in reverse osmosis, ultrafiltration, and microfiltration membranes prepared by phase inversion process, J. Colloid Interface Sci. 147 (1991) 307–315, doi:10.1016/0021-9797(91)90162-2.
[22] R.W. Field, G.K. Pearce, Critical, sustainable and threshold fluxes for membrane filtration with water industry applications, Adv. Colloid Interface Sci. 164 (2011) 38–44, doi:10.1016/j.cis.2010.12.008.
[23] A. Ilyas, M. Mertens, S. Oyaert, I.F.J. Vankelecom, Synthesis of patterned PVDF ultrafiltration membranes: spray-modified non-solvent induced phase separation, J. Membr. Sci. 612 (2020) 118383, doi:10.1016/j.memsci.2020.118383.
[24] M.-.J. Tang, M.-.L. Liu, D.-.A. Wang, D.-.D. Shao, H.-.J. Wang, Z. Cui, X.-.L. Cao, S.-.P. Sun, Precisely patterned nanostrand surface of cucurbituril[*n*]-based nanofiltration membranes for effective alcohol–water condensation, Nano Lett. 20 (2020) 2717–2723, doi:10.1021/acs.nanolett.0c00344.
[25] N.U. Barambu, M.R. Bilad, Y. Wibisono, J. Jaafar, T.M.I. Mahlia, A.L. Khan, Membrane surface patterning as a fouling mitigation strategy in liquid filtration: a review, Polym. Basel 11 (2019) 1687, doi:10.3390/polym11101687.
[26] J. Garcia-Ivars, M.-.I. Alcaina-Miranda, M.-.I. Iborra-Clar, J.-.A. Mendoza-Roca, L. Pastor-Alcañiz, Enhancement in hydrophilicity of different polymer phase-inversion ultrafiltration membranes by introducing PEG/Al2O3 nanoparticles, Sep. Purif. Technol. 128 (2014) 45–57, doi:10.1016/j.seppur.2014.03.012.
[27] Y. Ma, F. Shi, Z. Wang, M. Wu, J. Ma, C. Gao, Preparation and characterization of PSf/clay nanocomposite membranes with PEG 400 as a pore forming additive, Desalination 286 (2012) 131–137, doi:10.1016/j.desal.2011.10.040.
[28] L.-.S. Wan, Z.-.K. Xu, Z.-.G. Wang, Leaching of PVP from polyacrylonitrile/PVP blending membranes: a comparative study of asymmetric and dense membranes, J. Polym. Sci. Part B Polym. Phys. 44 (2006) 1490–1498, doi:10.1002/polb.20804.
[29] N.I. Mat Nawi, H.M. Chean, N. Shamsuddin, M.R. Bilad, T. Narkkun, K. Faungnawakij, A.L. Khan, Development of hydrophilic PVDF membrane using vapour induced phase separation method for produced water treatment, Membranes 10 (2020) 121, doi:10.3390/membranes10060121.
[30] A. Fahrina, N. Arahman, S. Mulyati, S. Aprilia, N.I. Mat Nawi, A. Aqsha, M.R. Bilad, R. Takagi, H. Matsuyama, Development of polyvinylidene fluoride membrane by incorporating bio-based ginger extract as additive, Polym. Basel 12 (2020) 2003, doi:10.3390/polym12092003.
[31] V. Discart, M.R. Bilad, R. Moorkens, H. Arafat, I.F.J. Vankelecom, Decreasing membrane fouling during Chlorella vulgaris broth filtration via membrane development and coagulant assisted filtration, Algal Res. 9 (2015) 55–64, doi:10.1016/j.algal.2015.02.029.
[32] N. Arahman, S. Mulyati, A. Fahrina, S. Muchtar, M. Yusuf, R. Takagi, H. Matsuyama, N.A.H. Nordin, M.R. Bilad, Improving water permeability of hydrophilic PVDF membrane prepared via blending with organic and inorganic additives for humic acid separation, Molecules 24 (2019) 4099, doi:10.3390/molecules24224099.
[33] H. Beygi, E.Z. Karimi, R. Farazi, F. Ebrahimi, A statistical approach to synthesis of functionally modified silica nanoparticles, J. Alloy. Compd. 654 (2016) 308–314, doi:10.1016/j.jallcom.2015.09.070.
[34] H. Wu, J. Mansouri, V. Chen, Silica nanoparticles as carriers of antifouling ligands for PVDF ultrafiltration membranes, J. Membr. Sci. 433 (2013) 135–151, doi:10.1016/j.memsci.2013.01.029.
[35] A. Bottino, Preparation and properties of novel organic–inorganic porous membranes, Sep. Purif. Technol. 22–23 (2001) 269–275, doi:10.1016/S1383-5866(00)00127-1.
[36] M.O. Mavukkandy, M.R. Bilad, J. Kujawa, S. Al-Gharabli, H.A. Arafat, On the effect of fumed silica particles on the structure, properties and application of PVDF membranes, Sep. Purif. Technol. 187 (2017) 365–373, doi:10.1016/j.seppur.2017.06.077.
[37] J. Huang, K. Zhang, K. Wang, Z. Xie, B. Ladewig, H. Wang, Fabrication of polyethersulfone-mesoporous silica nanocomposite ultrafiltration membranes with antifouling properties, J. Membr. Sci. 423–424 (2012) 362–370, doi:10.1016/j.memsci.2012.08.029.
[38] M. Baghbanzadeh, D. Rana, C.Q. Lan, T. Matsuura, Effects of hydrophilic silica nanoparticles and backing material in improving the structure and performance of VMD PVDF membranes, Sep. Purif. Technol. 157 (2016) 60–71, doi:10.1016/j.seppur.2015.11.029.
[39] M.R. Bilad, E. Guillen-Burrieza, M.O. Mavukkandy, F.A. Al Marzooqi, H.A. Arafat, Shrinkage, defect and membrane distillation performance of composite PVDF membranes, Desalination 376 (2015) 62–72, doi:10.1016/j.desal.2015.08.015.
[40] F.A. AlMarzooqi, M.R. Bilad, B. Mansoor, H.A. Arafat, A comparative study of image analysis and porometry techniques for characterization of porous membranes, J. Mater. Sci. 51 (2016) 2017–2032, doi:10.1007/s10853-015-9512-0.
[41] A. Eliseus, M.R. Bilad, N.A.H.M. Nordin, A.L. Khan, Z.A. Putra, M.D.H. Wirzal, M. Aslam, A. Aqsha, J. Jaafar, Two-way switch: maximizing productivity of tilted panel in membrane bioreactor, J. Environ. Manag. 228 (2018) 529–537, doi:10.1016/j.jenvman.2018.09.029.
[42] C. Van Goethem, M.M. Magboo, M. Mertens, M. Thijs, G. Koeckelberghs, I.F.J. Vankelecom, A scalable crosslinking method for PVDF-based nanofiltration membranes for use under extreme pH conditions, J. Membr. Sci. 611 (2020) 118274, doi:10.1016/j.memsci.2020.118274.
[43] C. Van Goethem, M. Mertens, I.F.J. Vankelecom, Crosslinked PVDF membranes for aqueous and extreme pH nanofiltration, J. Membr. Sci. 572 (2019) 489–495, doi:10.1016/j.memsci.2018.11.036.
[44] R. Al-Oweini, H. El-Rassy, Synthesis and characterization by FTIR spectroscopy of silica aerogels prepared using several Si(OR)4 and R″Si(OR′)3 precursors, J. Mol. Struct. 919 (2009) 140–145, doi:10.1016/j.molstruc.2008.08.025.
[45] N.O. Gopal, K.V. Narasimhulu, J.L. Rao, EPR, optical, infrared and Raman spectral studies of Actinolite mineral, Spectrochim. Acta. A. Mol. Biomol. Spectrosc. 60 (2004) 2441–2448, doi:10.1016/j.saa.2003.12.021.
[46] C. Liao, J. Zhao, P. Yu, H. Tong, Y. Luo, Synthesis and characterization of low content of different SiO2 materials composite poly (vinylidene fluoride) ultrafiltration membranes, Desalination 285 (2012) 117–122, doi:10.1016/j.desal.2011.09.042.
[47] S.-.H. Yoon, Membrane bioreactor processes: principles and applications, 2016. http://www.crcnetbase.com/isbn/9781482255843 (Accessed December 9, 2019).
[48] F. Meng, H. Zhang, F. Yang, S. Zhang, Y. Li, X. Zhang, Identification of activated sludge properties affecting membrane fouling in submerged membrane bioreactors, Sep. Purif. Technol. 51 (2006) 95–103, doi:10.1016/j.seppur.2006.01.002.